Multifunctional Control Algorithm for VSC-Based Grid-Connected Microgrid for Compensation Operation Modes

HAMED JOORABLI[1], GEVORK B GHAREHPETIAN[2,*], VAHID GHODS[1], AND MEHDI FALLAH[3]

[1] *Department of Electrical Engineering, Semnan Branch, Islamic Azad University, Semnan, Iran*
[2] *Department of Electrical Engineering, Amirkabir University of Technology, Tehran, Iran*
[3] *Faculty of Electrical and Computer Engineering, Sahand University of Technology, Tabriz, Iran*
[*] *Corresponding author email: grptian@aut.ac.ir*

Manuscript received 13 April, 2022; revised 29 June, 2023; accepted 7 July, 2023. Paper no. JEMT-2204-1379.

In some configurations, microgrid is connected to an AC grid via voltage source converters (VSCs), supplying local non-linear loads (NLLs) of the microgrid connected to the output of the VSC. In such condition, the produced current distortions of the NLLs may flow through the AC grid due to low impedance. Hence, the microgrid should compensate the current distortions, which have been generated by the NLLs. On the other hand, when the AC grid has voltage harmonics, they amplify the produced distortions of the NLLs. To harness these distortions, this paper proposes a new multifunctional control method of the grid connecting microgrid VSC, which can decompose the current distortions into two components originated by the NLLs, and other one by the AC grid voltage harmonics. Then, VSC-based grid-connected microgrid can operate in two compensation modes. The first operation mode includes the compensation of distortions only with considering NLLs contribution. While in the second mode, VSC tries to compensate the distortions with considering contributions of both NLLs and AC grid voltage harmonics. In this mode, the proposed method is able to limit the total harmonic distortion level of AC grid side current in the standard limitation (less than 5%). The effectiveness of the proposed control method is studied using the simulations and experiments.

keywords: *Microgrid, Distortions Compensation, Power Quality, Voltage Source Converter, Multifunctional Control Method*

http://dx.doi.org/10.22109/jemt.2023.337482.1379

NOMENCLATURE

n	Order of harmonic
$\delta(rad)$	Phase difference between PCC voltage and NLLs current
$\omega(rad/\sec)$	Grid angular frequency
τ	Transposition of the matrix
$V_{pcc}(v)$	Voltage of point of common coupling
$I_{NLLs}(A)$	Current of nonlinear loads
T	Park transformation
$V_{pcc-dq}(v)$	Voltage of point of common coupling in dq frame
$I_{NLLs-dq}(A)$	Current of nonlinear loads in dq frame
$P(t)$	Instantaneous power
γ	SOGI gain
$D(s), Q(s)$	Orthogonal signals generated by SOGI
s	Laplace domain operator
V_d, V_q	Voltage in dq frame
I_d, I_q	Current in dq frame
$Z_{MG}, Z_G(\Omega)$	Line impedance of microgrid and main grid

1. INTRODUCTION

There are various configurations of grid-connected microgrids. One of them can be seen in Fig. 1. As it can be seen in this figure, it has a non-linear load (NLL) connected to point of common

coupling (PCC) [1]. Considering the behavior of NLLs, one of the important issues of this structure is power quality improvement. The local non-linear loads (NLLs) are absorbing a wide spectrum of current harmonics. But, when the AC main grid contains voltage harmonics, they can affect the spectrum of the current harmonics of the NLLs, and thereby, increase the total harmonic distortion (THD) [2]. For the structure presented in Fig. 1, many solutions have been presented for controlling VSCs in different applications. For example, for renewable energy sources (RESs), the converters control reactive power to adjust voltages within an acceptance range, while they also deliver active power to the power system [3]. In [4] different methods have been suggested for controlling of active and reactive powers flow in a single-phase microgrid when it operates in grid-connected mode. To this end, proposed methods have been developed based on dq frame calculation, and their performance has been compared with other methods considering different condition. However, this paper addresses active and reactive powers flow in single-phase system, but it doesn't evaluate the proposed methods in the presence of distortions. Among all methods, droop control method is an effective method to control a VSC-based microgrid for independently delivering active and reactive powers from DC side to AC side. Although, it has been widely accepted that the droop control only takes effect at the fundamental frequency and has little influence on the mentioned performance in a distorted environment [5].

Moreover, there are many papers focusing on the reactive power control, which include unity power factor method, active power-dependent method, dynamic operational method, etc. The aim of the unity power factor method is to have converters without any reactive power injection. This method is in complete compliance with the previous version of IEEE Standard 1547 and UL1741, which specify that distributed resources should not actively regulate voltage at PCC [6]. It is worthy to be noted that in some cases such as lack or shortage of power in renewable resources, the performance of this method is not suitable as the control unit of microgrid. The active power-dependent method has been proposed by German grid codes [7]. This solution adjusts the reactive power flow back to the grid based on active power output of the converter; thus, it provides a kind of voltage regulation according to output active power variations. In [8], a dynamic operational method is presented, where the converter could generate inductive or capacitive reactive powers at different voltage levels. This method can operate in three states including normal and voltage fluctuating states. In fluctuating state, reactive power is modulated in order to mitigate voltage fluctuations caused by transient movement. So, it is obvious that this method could not contribute to solve power quality issues, which are stem from main grid side or local loads. In [9] a novel secondary control strategy for the VSC-based microgrid in suggested. This strategy restores the voltage and frequency deviations by utilizing only local variables with high bandwidth. However, this control method could handle voltage and frequency deviations, but its performance can be influenced by noise and distortions due to its high bandwidth. A multifunctional control scheme to control the VSC-based grid-connected microgrid has been proposed using instantaneous symmetrical components theory in [10]. Based on this method, VSC-based microgrid operates in three modes including (1) as a bidirectional power sharing converter to control power flow from DC side to AC side and vice versa, (2) for damping the oscillations using filter in the control algorithm, and (3) as a power quality compensator to mitigate current harmonics of non-linear loads and reactive power compensation in PCC to purify main grid from any distortions with unit power factor. It seems that this method is suitable for VSC-based microgrid due to its multifunctional performance, however, the performance of this method has not been evaluated with considering PCC voltage harmonics. The state-of-art power system support functions are summarized in [11] for the purpose of enhancing operations in grid-connected VSC-based microgrids. In this paper a useful review has been carried out with associated to power system support functions including reactive power control, fault ride-through and harmonic compensation. This paper emphasizes that developing new control methods with multifunctional operation abilities is very important for avoiding extra cost and high reliability. In pertaining to harmonic mitigation, flexible control of grid-connected VSC-based microgrid may be utilized to offer the possibility of power quality improvement. As a result, the harmonic compensation function could be integrated with the control scheme by modifying the control strategies [12]. This is especially attractive considering that DC side of VSC does not always act at full capacity, and the available capacity can be used to realize harmonic compensation without additional costs.

Also, some papers have focused on the mitigation of the harmonics of local non-linear loads, using the multi-resonance controller (MRC) based harmonic elimination method, repetitive controller (RC) based harmonic elimination method, optimized model predictive control (MPC) method, etc. The MRC method could easily compensate low-order harmonics of NLLs, though the discretization of multiple resonant controllers would result in a heavy calculation burden, and the fundamental frequency variation would affect the performance [13]. In [14], a new control method is proposed for microgrid-connected voltage source converters (VSCs), which generally contain voltage and current control loops. The voltage of the point of common coupling (PCC) is analyzed by recursive least squares (RLS) algorithm and its fundamental positive symmetric components are extracted by the voltage control loop. Using the fundamental positive symmetric component, the required active and reactive powers are injected into the main grid via the microgrid-connected VSC without any distortions. In [15], a computational method has been used based on the recursive least squares with the variable forgetting factor (VFF-RLS). The prominent features of the proposed method are its high accuracy and speed, as well as identification with a low rate of signal samples. The main aim of the proposed method is to identify the contribution and extent of harmonics and unbalanced in a Microgrid equipped with advanced metering infrastructure (AMI).

In [16], a resonant controller with self-tuned gains is presented for improvement of VSC-based microgrid in the presence of voltage and frequency variations. This method imposes a constant sampling time which allows controllers to be used in variable frequency environments. Nevertheless, the controllers with self-tuned gains can solve the disadvantages of voltage and frequency variations, but it can lead to decreasing the stability of whole control system due to its parameter changing. In [17], resonant controller guidelines are given to increase stability margins and to eliminate typical three-phase harmonics ±6n+1 with n a natural number. This work helps the overall control performance of a resonant controller where this design can be used to opt the controller parameters. A detailed analysis about the model and control parameters design is made, and therefore, the procedure may be followed for any system that needs a resonant controller. The repetitive controller method could reject the harmonics of NLLs below the Nyquist frequency using a simple

phase compensator. This method could remove the harmonics using less calculation than the resonant controller method, but it presented a much slower dynamic response than the resonant controller method [18]. Meanwhile, in [19] a model predictive control method is employed for a distorted environment. The control dynamic tracks references quickly and accurately. However, the variable switching frequency makes the filter parameter design more difficult, and the computation effort is higher, since all the states need to be tested before to select the best control actuation to minimize a specified cost function. Besides, the MPC method could mitigate the harmonics of NLLs, but the same as the MRC and RC methods, it had heavy calculations. Nevertheless, all of these control methods were more beneficial than employing extra devices such as shunt active power filter (APF) or passive power filter (PPF), imposing more costs, complexity, and maintenance [20]. As mentioned before, another important point is the effect of the main grid voltage harmonics on the current harmonics' elimination of NLLs. This phenomenon influences the performance of the control system, for example, the phase-locked loop (PLL) can be affected by distortions. In [21], a complete review of PLLs has been presented including the stationary reference frame PLL ($\alpha\beta PLL$) and a decoupled double synchronous reference frame PLL (ddsrfPLL). Also, it has proposed a new PLL, called decoupled stationary reference frame PLL ($d\alpha\beta PLL$), to improve the performance under non-ideal conditions. The $d\alpha\beta PLL$ has a suitable performance in the presence of voltage distortions, but it has a sophisticated structure [22].

In the presence of the background voltage harmonics, the absorbed distortions of the NLLs will increase in comparison with ideal conditions which is without voltage harmonics. In other words, the microgrid is in charge of the distortion's compensation of the NLLs, however, these distortions consist of two parts. The first part of the distortions is related to the behavior of the NLLs. The microgrid should compensate these distortions because of its responsibility. The second part of the distortions is generated due to the main grid voltage harmonics, and as a result, this part should not be compensated by the microgrid. Then, the microgrid can operate in two modes. In the first mode, it just compensates the first part of the distortions, and neglects the effect of the main grid voltage harmonics. In the second mode, it participates in the compensation of the distortion's contributions of both NLLs and the main grid voltage harmonics. The first mode can be called as the partial compensation mode, and the second mode can be termed as the full compensation mode. Note that the full compensation mode can have an economic benefit for the microgrid, in case of participation in ancillary service market of the grid. Accordingly, this paper suggests a novel multifunctional control strategy for the grid connecting microgrid converter considering the contribution of the grid voltage harmonics. To this end, the proposed control method calculates the total distortion powers of the NLLs absorbed by them, and then it separates the contribution of the NLLs as well as the contribution of the main grid voltage harmonics.

The proposed control method can enhance the power quality in two compensation modes. It uses the power-based calculation approach for the compensation of distortions instead of calculating harmonics extraction. Note that in both compensation modes the microgrid transfers the required active and reactive power simultaneously. In addition, for the proper synchronization of the microgrid with the polluted main grid, a second-order generation integrator frequency locked loop (SOGI-FLL) is exploited due to its prominent features such as easy implementation and the ability of reference phase tracking in the presence of voltage harmonics. In fact, the purpose of paper is identification of origin of distortions at PCC. In other words, these distortions can be generated by non-linear loads and background voltage harmonics of the grid. To this end, the proposed control method utilizes the instantaneous power theory for segregation of contribution of the non-linear loads and the main grid. After identifying the origin of distortions, the proposed control method can compensate the distortion contribution of the non-linear loads, the main grid or both of them in different compensation modes. Thanks to computation based on the instantaneous power theory, the proposed control method has a simple structure with low calculation volume, and as a result, its implementation can be done by popular microcontroller. In addition, this low calculation volume leads to fast response with high accuracy. As it will be shown in simulation and experiment results the suggested control method can reduce THD of current within standard limitation in full compensation mode. Moreover, in the case that it does not need to compensate the contribution of main grid voltage harmonic, it can only compensate contribution of NLLs with high accuracy in both segregation of contributions and compensation of target contribution.

The rest of this paper is arranged as follows. Section 2 deals with the distortion of NLLs. Section 3 proposes the multifunctional control method. Sections 4 and 5 provide the simulation and experimental results for validation of the proposed method. Eventually, section 6 concludes the paper.

2. DISTORTIONS OF NLLS

As can be seen from Fig. 1, NLLs are usually connected to the AC side of VSC, and current distortions generated by them, may flow via the AC grid. Hence, the power quality of the main grid decreases. As mentioned, if the main grid contains the background voltage harmonics, they can affect the current distortions of the NLLs. So, the distortions absorbed by the NLLs are divided into two parts. The first part, regardless of the background voltage harmonic, is termed as the distortion's contribution of the NLLs (DC-NLLs), and the other one, including the NLLs and the grid harmonics, is named as the distortion's contribution of the grid (DC-G). Here, the microgrid can operate in three modes: 1. it only transfers the active and reactive powers without considering the DC-NLLs and DC-G, 2. it can carry over both active and reactive powers, and simultaneously compensates the DC-NLLs, and 3. it can accomplish the power transfers, and at the same time, it compensates both the DC-NLLs and DC-G. The frequency mapping of PCC voltage, as well as NLLs current can be exploited in time domain and rotational frame (dq) for calculating instantaneous powers. By neglecting the background voltage harmonics, the vectors of the PCC voltage, as well as the NLLs current can be stated as (1) and (2) in the time domain, respectively

$$[V_{pcc}] = \begin{bmatrix} v_a \\ v_b \\ v_c \end{bmatrix} = \begin{bmatrix} v_a \sin(\omega t) \\ v_b \sin(\omega t - 2\pi/3) \\ v_c \sin(\omega t + 2\pi/3) \end{bmatrix} \quad \textbf{(1)}$$

$$[I_{NLLs}] = \begin{bmatrix} i_a \\ i_b \\ i_c \end{bmatrix} = \begin{bmatrix} \sum_{n-1}^{\infty} I_{an} \sin(n\omega t - \delta_n) \\ \sum_{n-1}^{\infty} I_{bn} \sin(n\omega t - \delta_n - 2\pi/3) \\ \sum_{n-1}^{\infty} I_{cn} \sin(n\omega t - \delta_n + 2\pi/3) \end{bmatrix} \quad \textbf{(2)}$$

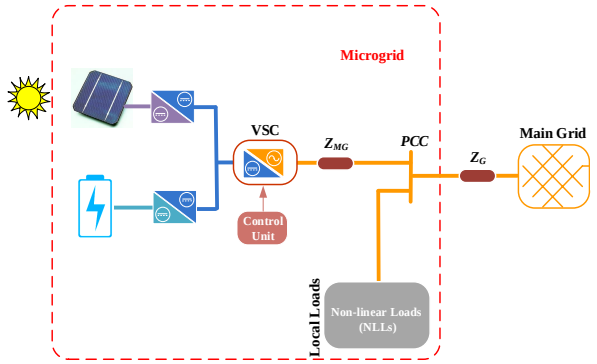

Fig. 1. The studied microgrid

where, n is order of harmonic, δ represents the phase difference between PCC voltage and NLLs current, and ω denotes the grid angular frequency. Equations (1) and (2) can be transferred to the rotating frame by (3) and (4).

$$[V_{pcc-dq}] = [T].[V_{pcc}] \quad \textbf{(3)}$$

$$[I_{NLLs-dq}] = [T].[I_{NLLs}] \quad \textbf{(4)}$$

where, T is the Park transformation matrix, which is obtained as (5).

$$[T] = \sqrt{\frac{2}{3}} \begin{bmatrix} \cos(\omega t) & \cos(\omega t - 2\pi/3) & \cos(\omega t + 2\pi/3) \\ -\sin(\omega t) & -\sin(\omega t - 2\pi/3) & -\sin(\omega t + 2\pi/3) \\ \sqrt{2}/2 & \sqrt{2}/2 & \sqrt{2}/2 \end{bmatrix} \quad \textbf{(5)}$$

Accordingly, the instantaneous power can be computed by (6).

$$P(t) = [V_{pcc}]^{\tau}.[I_{NLLs}] = [V_{pcc-dq}]^{\tau}.[I_{NLLs-dq}]^{\tau} \quad \textbf{(6)}$$

where, the superscript τ denotes the transposition of the matrix. Considering the main grid voltage harmonics as (7), the instantaneous power can be calculated by (3) and (6) in the time domain and dq rotational frame.

$$[V_{pcc}] = \begin{bmatrix} v_a \\ v_b \\ v_c \end{bmatrix} = \begin{bmatrix} \sum_{n-1}^{\infty} V_{an} \sin(n\omega t) \\ \sum_{n-1}^{\infty} V_{bn} \sin(n\omega t - 2\pi/3) \\ \sum_{n-1}^{\infty} V_{cn} \sin(n\omega t + 2\pi/3) \end{bmatrix} \quad \textbf{(7)}$$

For more clarity, the frequency mapping of the PCC voltage and the NLLs current are demonstrated in Fig. 2 based on (6). Note that in Fig. 2(a), the main grid voltage is given by (1) and it is free of harmonics, while in Fig. 2(b), (7) is assumed to be the main grid voltage, which contains background voltage harmonics. Based on Fig. 2(a), and neglecting the background voltage harmonics, the NLLs consume the DC power (Pdc) and the even-orders of the power (i.e.,$P_{2\omega(rad/\sec)}$, $P'_{2m\omega(rad/\sec)}$, $\sum_{m=1}^{\infty} P''_{2m\omega(rad/\sec)}$,and etc). However, in the presence of the background voltage harmonics, it is obvious that the NLLs absorb the several components of the DC power (i.e, P_{dc}, P'_{dc}, P''_{dc},etc) as well as other even-orders of the power(i.e,P_{dc}, P'_{dc}, $\sum_{m=1}^{\infty} P_{2m\omega(rad/\sec)}$, $\sum_{m=1}^{\infty} P'_{2m\omega(rad/\sec)}$, and etc.), as illustrated in Fig. 2(b). Hence, regarding power consumption, the background voltage harmonics contribute to higher values of DC power and other components of the powers. In other words, it can be deduced that the DC-NLLs produce the distortion power components as (8), with the sum of the DC-NLLs and DC-G being equal to (9). Eventually, the DC-G can be computed by (8), (9) and (10), as follows:

$$P_{DC-NLLs} = \sum_{m=1}^{\infty} (P_{2m\omega(rad/\sec)} + P'_{2m\omega(rad/\sec)}) \quad \textbf{(8)}$$

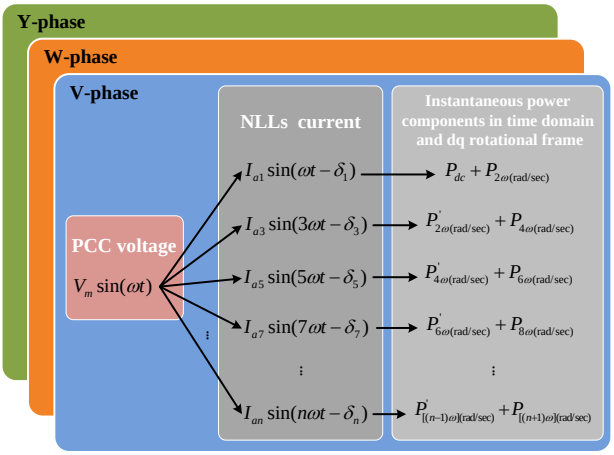

(a)

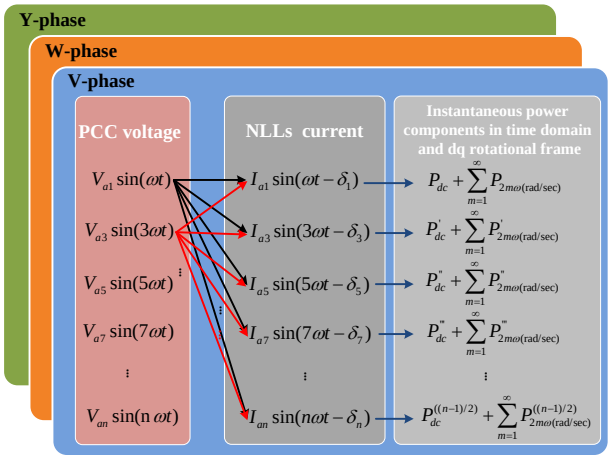

(b)

Fig. 2. The frequency mapping of PCC voltage and NLLs current (a) without background voltage harmonics, (b) in the presence of background voltage harmonics

$$P_{Total} = P'_{dc} + P''_{dc} + P'''_{dc} + ... + \sum_{m=1}^{\infty} (P_{2m\omega(rad/\sec)} + P'_{2m\omega(rad/\sec)} + P''_{2m\omega(rad/\sec)} + ...) \quad \textbf{(9)}$$

$$P_{DC-G} = P_{Total} - P_{DC-NLLs} = P'_{dc} + P''_{dc} + ... + \sum_{m=1}^{\infty} (P''_{2m\omega(rad/\sec)} + P'''_{2m\omega(rad/\sec)} + ...) \quad (10)$$

Note that in (10), the distorted DC powers (P'_{dc},P''_{dc} and etc.) are in accordance with the phase difference between the same order harmonics of PCC voltage and the NLLs current. Comparison of DC and oscillating terms of (10) is given in (11). Based on (11), the PDC-PS can be approximately obtained by (12).

$$P'_{dc} + P''_{dc} + ... << \sum_{m=1}^{\infty} (P''_{2m\omega(rad/\sec)} + P'''_{2m\omega(rad/\sec)} + ...) \quad (11)$$

$$P_{DC-G} \approx \sum_{m=1}^{\infty} (P''_{2m\omega(rad/\sec)} + P'''_{2m\omega(rad/\sec)} + ...) \quad (12)$$

The aforementioned assessment proves that the background voltage harmonics has an adverse effect on the absorbed power by the NLLs, and at the same time, the distortions contribution of the main grid can be detected by evaluating the absorbed power of the NLLs. Hence, in this article, a novel multifunctional control approach is introduced for controlling the grid-connecting microgrid VSC, in order to determine the distortions contribution of the main grid voltage harmonics. Meanwhile, the microgrid VSC can operate in full compensation mode, and as a result, it can compensate the distortions of the background voltage harmonics and the NLLs current.

3. PROPOSED MULTIFUNCTIONAL CONTROL METHOD

The proposed multifunctional control strategy has been displayed in Fig. 3. According to this sketch, the suggested method consists of two control layers. Note that Fig. 3 has been divided into Fig. 3(a), 3(b) and 3(c), which shows overall configuration of control and power sections, compensation mode in DC-NLLs mode and full compensation mode, respectively. The proposed method can completely segregate the contribution of non-linear loads distortions from the contribution of distorted main grid. Then it can compensate the contributions of both or each of them. This method is based on the instantaneous power theory, which computes distortion powers, and exploits them to generate the reference signals. For proper synchronization of the VSC with the main grid, the SOGI-FLL is embedded in the proposed structure. This type of the PLL can detect the reference phase of grid in the presence of background voltage harmonics, as well as, when a disturbance occurs in the grid such as frequency oscillations or phase jumping. Indeed, the SOGI-FLL is a tight band filter, which passes fundamental component of its input signal. The sketch of SOGI-FLL is demonstrated in Fig. 4(a). Accordingly, SOGI-FLL can produce two orthogonal signals in accordance with the fundamental frequency, where the fundamental frequency is tracked by FLL. The transfer functions of the generated orthogonal signals are given by (13) and (14).

$$D(s) = \frac{V_d}{V_{PCC}}(s) = \frac{\gamma\omega' s}{s^2 + \omega'^2} \quad (13)$$

$$Q(s) = \frac{V_d}{V_{PCC}}(s) = \frac{\gamma\omega'^2}{s^2 + \omega'^2} \quad (14)$$

where, Vd and Vq are the output orthogonal signals. Also, γ and ω' present the gain of SOGI-FLL and its resonance filter, respectively. Finally, s is the frequency domain operator. Note that when the main grid is free of any frequency oscillation, ω' is equal to ω. The bode plot of aforementioned transfer functions is demonstrated in Fig. 4(b). Here, it is assumed that and are equal to 2 and 314 (rad/sec), respectively. The key point is the effect ofγ on the performance of SOGI-FLL, as can be seen in Fig. 4(b). According to this figure, (13) and (14), the variation of γ leads to altered the bandwidth of SOGI-FLL. In other words, increasing γ enhances the bandwidth, and vice versa. Regarding dynamic response, choosing a large value of γ is effective, which will cause a vast bandwidth. On the other hands, this selection leads to the generation of poor-quality orthogonal signals when there are background voltage harmonics. As the detrimental components of the voltage can pass to the output signals. Hence, a trade-off should be established between the precision and speed of response for selecting . The gain of SOGI-FLL shifts the bode plot vertically, while moves the bode plot horizontally in accordance with the determined resonance frequency by the FLL. The reference phase of the main grid can be obtained as (15).

$$\omega t = \tan^{-1}(\frac{v_d}{v_q}) \quad (15)$$

where, Vd and Vq present the inverse Laplace transform of Vd and Vq, respectively. Based on (15), this reference phase can be used in park transformation and its inverse transformation. Further, the sinusoidal wave generation unit produces the virtual pure three-phase voltage as (16).

$$[\hat{V}_{PCC}] = \begin{bmatrix} \hat{v}_a \\ \hat{v}_b \\ \hat{v}_c \end{bmatrix} = \begin{bmatrix} \hat{v}_a \sin(\omega t) \\ \hat{v}_b \sin(\omega t - 2\pi/3) \\ \hat{v}_c \sin(\omega t + 2\pi/3) \end{bmatrix} \quad (16)$$

In the first control layer, the voltages of DC bus, and VSC output are adjusted. Then the required active and reactive powers are calculated using their reference values. For this purpose, the DC bus voltage of microgrid is compared with its setpoint value, and at the same time, the output AC voltage of VSC is compared with its setpoint value. The obtained error signals are crossed via the PI controllers for their regulation, and eventually, the output signals of PI controllers are added to the setpoint powers values. Accordingly, the reference current in dq frame (Iinj-d and Iinj-q) can be gained using (17) and (18), which has been stated by (19).

$$P_{inj} = 3(\hat{V}_{PCC-d} I_{inj-d} + \hat{V}_{PCC-q} I_{inj-q}) \quad (17)$$

$$Q_{inj} = 3(\hat{V}_{PCC-d} I_{inj-q} - \hat{V}_{PCC-q} I_{inj-d}) \quad (18)$$

$$\begin{bmatrix} I_{inj-d} \\ I_{inj-q} \end{bmatrix} = \frac{1/3}{\hat{V}^2_{PCC-d} + \hat{V}^2_{PCC-q}} \begin{bmatrix} \hat{V}_{PCC-d} & \hat{V}_{PCC-q} \\ \hat{V}_{PCC-q} & -\hat{V}_{PCC-d} \end{bmatrix} \begin{bmatrix} P_{inj} \\ Q_{inj} \end{bmatrix} \quad (19)$$

where, $\hat{V}_{PCC-d}$ $\hat{V}_{PCC-q}$ and can be gained by applying (5) on (16); hence, the obtained reference current used in (17) and (18) will be pursuant to the fundamental of main grid voltage, which is one of the advantages of suggested control strategy. In fact, based on this control layer the VSC tries to deliver active and reactive powers from DC side to the AC side with minimum THD level without considering the main grid voltage harmonics at PCC. Also, the aim of suggested second control layer is compensating for DC-NLLs while considering the background voltage harmonics. Notably, it can compensate both the DC-NLLs and

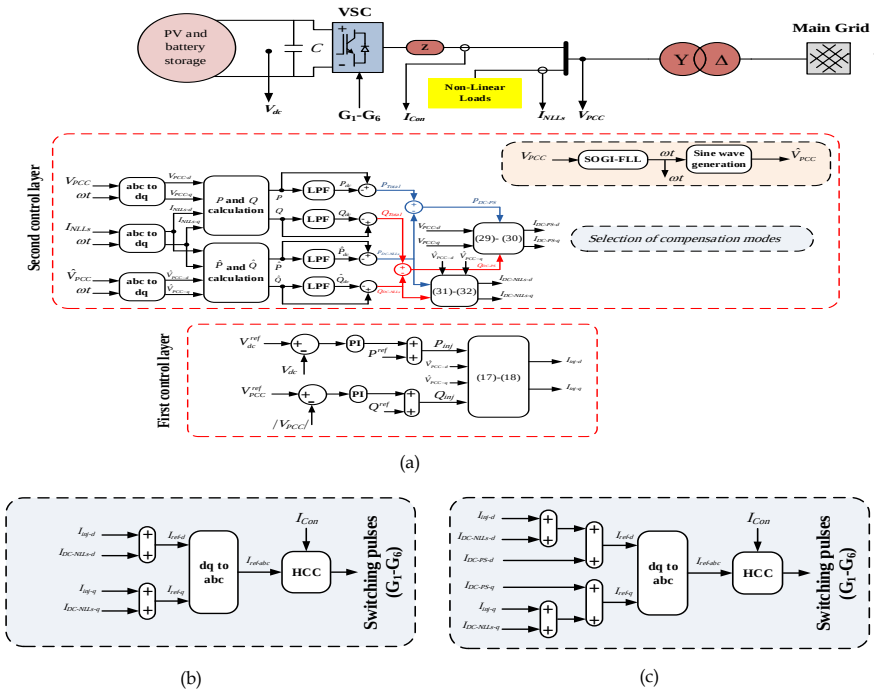

Fig. 3. (a) The proposed multifunctional control method for grid-connecting microgrid VSC, (b) compensation mode for DC-NLLs and (b) compensation mode for DC-NLLs + DC-G (full compensation mode)

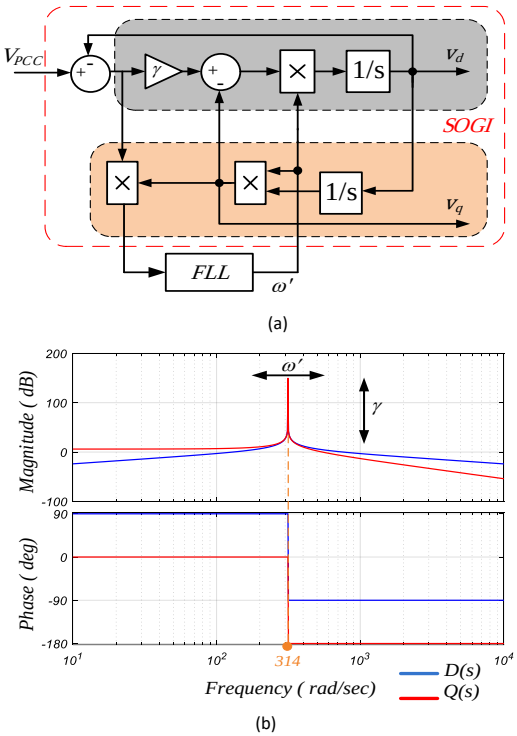

Fig. 4. (a) SOGI-FLL, and (b) the bode plot of D(s) and Q(s)

DC-G in the full compensation mode. According to the mentioned approach in the previous section, PCC voltage (V_{PCC}), current of the NLLs (I_{NNLs}), and virtual PCC voltage ($\hat{V}_{PCC}$) are transferred to dq frame by employing the Park transformation. Then, the powers are computed as (20)-(23).

$$P = P_{dc} + \tilde{P} = 3(V_{PCC-d}I_{NLLs-d} + V_{PCC-q}I_{NLLs-q}) \quad \textbf{(20)}$$

$$Q = Q_{dc} + \tilde{Q} = 3(V_{PCC-d}I_{NLLs-q} - V_{PCC-q}I_{NLLs-d}) \quad \textbf{(21)}$$

$$\hat{P} = \hat{P}_{dc} + \tilde{\hat{P}} = 3(\hat{V}_{PCC-d}I_{NLLs-d} + \hat{V}_{PCC-q}I_{NLLs-q}) \quad \textbf{(22)}$$

$$\hat{Q} = \hat{Q}_{dc} + \tilde{\hat{Q}} = 3(\hat{V}_{PCC-d}I_{NLLs-q} - \hat{V}_{PCC-q}I_{NLLs-d}) \quad \textbf{(23)}$$

Note that (20) and (21) denote the absorbed powers by NLLs in the presence of background voltage harmonics, while (22) and (23) express them after ignoring the background voltage harmonics. In addition, for both conditions, the absorbed powers consist of DC and oscillation parts, which are identified by dc subscript and tilde superscript, respectively. Accordingly, for separating these two parts, low pass filters (LPFs) are utilized for all powers, whereby the total active and reactive oscillating powers can be obtained as (24) and (25). It is worthy to be noted that several types of LPF can be employed to separate DC part from oscillation part such as Butterworth LPF and wavelet-based LPF. In [23] a complete review has been done on the performance of LPF for achieving a suitable response in terms of high accuracy and low delay. On the other hands, the key point is that (24) and (25) illustrate the distortion powers absorbed by the NLLs, considering the background voltage harmonics. Thanks to the virtual PCC voltage, (26) and (27) only provide the distortion

powers absorbed by NLLs without considering the background voltage harmonics.

$$P_{Total} = P - P_{dc} \quad (24)$$

$$Q_{Total} = Q - Q_{dc} \quad (25)$$

$$P_{DC-NLLs} = \tilde{P} - \hat{P}_{dc} \quad (26)$$

$$Q_{DC-NLLs} = \hat{Q} - \hat{Q}_{dc} \quad (27)$$

$$P_{DC-G} = P_{Total} - P_{DC-NLLs} = (P - \hat{P}_{dc}) - (P_{dc} - \hat{P}_{dc}) \quad (28)$$

As a result, (24) and (26), as well as (25) and (27) can be employed for the extraction of main grid voltage harmonics contribution on the absorbed distortions of NLLs. For this purpose, by subtracting (24) and (26), as well as (25) and (27), the distortions contribution of the main grid can be achieved as (28) and (29).

$$Q_{DC-G} = Q_{Total} - Q_{DC-NLLs} = (Q - \hat{Q}_{dc}) - (Q_{dc} - \hat{Q}_{dc}) \quad (29)$$

Finally, the reference current (IDC-G-d, IDC-G-q) in accordance with the contribution of the main grid voltage harmonics can be obtained by (30) and (31) in dq frame, which has been demonstrated as (32). Note that the reason to use VPCC in dq frame in (30) and (31) is to find current which is responsible for distortion powers at PCC.

$$P_{DC-G} = 3(V_{PCC-d} I_{DC-G-d} + V_{PCC-q} I_{DC-G-q}) \quad (30)$$

$$Q_{DC-G} = 3(V_{PCC-d} I_{DC-G-q} - V_{PCC-q} I_{DC-G-d}) \quad (31)$$

Simultaneously, for compensation of the distortion's contribution of the NLLs, similar to (30) and (31), the current of NLLs distortion powers (without considering the main grid voltage harmonics) in dq frame can be calculated using (26), (27) and generated virtual PCC voltage by SOGI-FLL as (33) and (34). Finally, current can be obtained in the matrix form as (35).

$$\begin{bmatrix} I_{DC-G-d} \\ I_{DC-G-q} \end{bmatrix} = \frac{1/3}{{V_{PCC-d}}^2 + {V_{PCC-q}}^2} \begin{bmatrix} V_{PCC-d} & V_{PCC-q} \\ V_{PCC-q} & -V_{PCC-d} \end{bmatrix} * \begin{bmatrix} P_{DC-G} \\ Q_{DC-G} \end{bmatrix} \quad (32)$$

$$P_{DC-NLLs} = 3(\hat{V}_{PCC-d} I_{DC-NLLs-d} + \hat{V}_{PCC-q} I_{DC-NLLs-q}) \quad (33)$$

$$Q_{DC-NLLS} = 3(\hat{V}_{PCC-d} I_{DC-NLLs-q} + \hat{V}_{PCC-q} I_{DC-NLLs-d}) \quad (34)$$

$$\begin{bmatrix} I_{DC-NLLs-d} \\ I_{DC-NLLs-q} \end{bmatrix} = \frac{1/3}{\hat{V}^2_{PCC-d} + \hat{V}^2_{PCC-q}} \begin{bmatrix} \hat{V}_{PCC-d} & \hat{V}_{PCC-q} \\ \hat{V}_{PCC-q} & -\hat{V}_{PCC-d} \end{bmatrix} * \begin{bmatrix} P_{DC-NLLs} \\ Q_{DC-NLLs} \end{bmatrix} \quad (35)$$

According to the aforementioned explanations, the grid-connecting VSC can operate in two different modes. In the first mode, equations including (17), (18), (31) and (32) are used to achieve the reference current. By solving (17) and (18), as well as (33) and (34), the reference current can be gained through their summation in dq frame. This mode provides the DC-NLLs compensation mode, so in this mode DC-NLLs are mitigated by the VSC without considering the main grid voltage harmonics. Also, the proposed control method can eliminate the DC-G, which is generated by the background voltage harmonic. For this purpose, the results of (30) and (31) will be added to the reference current that obtained in the DC-NLLs compensation mode, then the full compensation mode will be gained. In full compensation mode, the grid-connecting microgrid VSC can deliver the required powers, and simultaneously compensates both DC-NLLs and DC-G. Note that the reference current calculated in both modes should be transferred into the time domain via the inverse Park transformation. Finally, by applying the hysteresis current controller (HCC), suitable switching pulses are provided for the VSC. The reference current signals are demonstrated by (36) and (37) for the DC-NLLs and full compensation modes, respectively, where T-1 is the inverse Park transformation.

$$\begin{bmatrix} I_{ref-a} \\ I_{ref-b} \\ I_{ref-c} \end{bmatrix} = T^{-1}. \begin{bmatrix} I_{DC-NLLs-d} + I_{inj-d} \\ I_{DC-NLLs-q} + I_{inj-q} \\ 0 \end{bmatrix} \quad (36)$$

$$\begin{bmatrix} I_{ref-a} \\ I_{ref-b} \\ I_{ref-c} \end{bmatrix} = T^{-1}. \begin{bmatrix} I_{DC-G-d} + I_{DC-NLLs-d} + I_{inj-d} \\ I_{DC-G-q} + I_{DC-NLLs-q} + I_{inj-q} \\ 0 \end{bmatrix} \quad (37)$$

4. SIMULATION RESULTS

The effectiveness of the suggested multifunctional control strategy is investigated by the MATLAB software. The system is exhibited in Fig. 5, which involves a grid-connecting VSC, local non-linear loads (NLLs), and AC grid containing voltage harmonics. Note that in this figure, the NLLs are modeled as a diode rectifier with L_{NLLs}, R_{NLLs} and C_{NLLs} on DC side. Other parameters of the studied system have been provided in Table 1. Referring to Fig. 3, the first control layer in the suggested

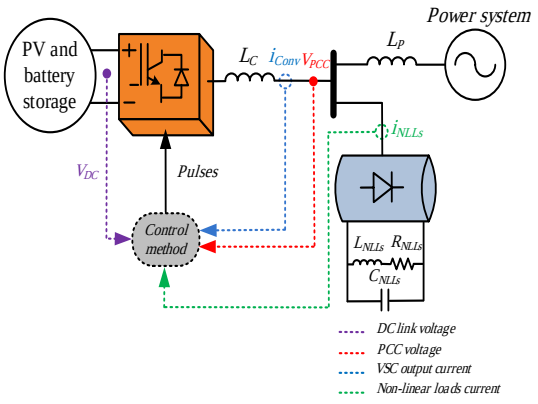

Fig. 5. The studied system

control approach tries to keep the DC bus voltage of microgrid in a fixed value without any fluctuation, so it can be assumed

Table 1. The parameters of studied system

Parameters	Definition	Value
f	Main grid frequency	50 Hz
LC	Inductance of the VSC output	5 mH
VrefPCC	PCC voltage	400 V
LNLLs, RNLLs and CNLLs	Equivalent inductance, resistance and capacitance of the non-linear loads	10 mH, 25 W and 500 mF
LP	Inductance of the main grid	1 mH
C	DC-link capacitance	4 mF
Pref and Qref	Reference values of the injected powers	25 kW and 500 VAR
g	SOGI-FLL gain	2
VrefDC	DC Voltage reference	750 V
ki and kp	Parameters of PI controller	0.1 and 1.6
fc and n	Cut-off frequency and order of LPF	30 Hz and 2

that the DC bus of microgrid is constant. The waveform of PCC voltage is demonstrated in Fig. 6, which contains 3rd and 5th order harmonics with values of 0.12 pu and 0.07 pu, respectively. According to the explained frequency mapping of the PCC voltage and NLLs current, these voltage harmonics can generate extra distortions, which are not in accordance with the NLLs. As mentioned before, the proposed multifunctional control method can separate the distortions contribution of NLLs from the contribution of PCC voltage harmonics. It can also compensate them in different compensation modes. The spectrum analysis of PCC voltage shows that its THD value is equal to 13.9%. Note that these background voltage harmonics can cause remarkable distortions. For example, if this PCC voltage is applied to a linear load, this load approximately consumes 19% distortion power more than that of the same load in case of having pure sinusoidal PCC voltage. As can be seen in Fig. 7(c), it is obvious that the

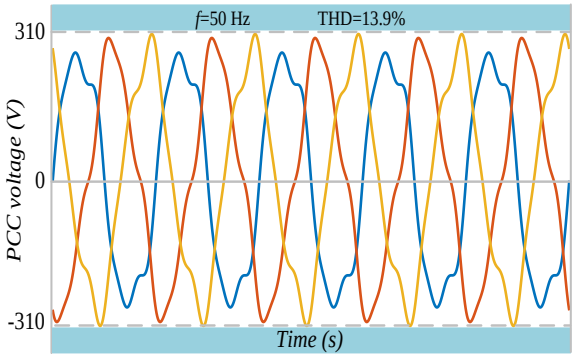

Fig. 6. PCC voltage with 3rd and 5th order harmonics

background voltage harmonics have a vital role in the degree of distortions of NLLs current. In particular, the harmonic orders of 3rd, 5th, 13th, and 19th increase the distortions of polluted PCC voltage. In other words, the PCC voltage harmonics lead to elevated THD of NLLs current from 26.5% to 32.6%, while their fundamental component is approximately constant. Hence, the distortion components of NLLs current will increase by 1.22 A based on Fig. 7(a) and 7(c), which is imposed by the background voltage harmonics. On the other hands, when the PCC voltage is considered to be free of harmonics, the distortion components of NLLs current will be equal to 5.3 A based on Fig. 7(b) and 7(c). Accordingly, the total distortion of NLLs current in the presence of PCC voltage harmonics are equal to 6.52 A. In this situation, if the grid-connecting VSC is not equipped with the compensation control loops, all the mentioned components tend to flow via the AC grid because of grid's small impedance. As a result, the proposed multifunctional control method not only compensates these distortions, but also it can distinguish between DC-NLLs and DC-G. So, the suggested control strategy only compensates the DC-NLLs in the DC-NLLs compensation mode, and both of them in the full compensation mode. The effectiveness of proposed multifunctional control approach has been assessed in the following section.

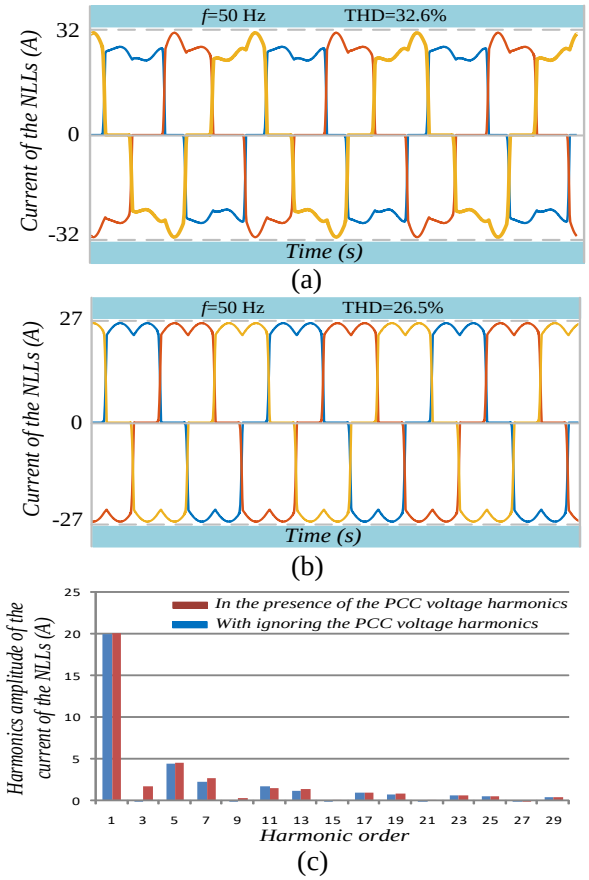

Fig. 7. Current waveform of NLLs (a) in the presence of PCC voltage harmonics, (b) without PCC voltage harmonics, and (c) the spectrum analysis of current waveform of NLLs

A. DC-NLLs Compensation Mode

In this mode, the grid-connecting VSC only tries to suppress the distortions contribution of the NLLs. Further, the microgrid VSC transfers the powers between DC and AC sides, simultaneously. Total distortion powers of NLLs are depicted in Fig. 8(a), considering the PCC voltage harmonics and absorbed by NLLs. On the other hand, by subtracting the distortions contribution of the main grid (DC-G) from the total distortion powers, produced by PCC voltage harmonics, DC-NLLs can be achieved as shown in Fig. 8(b). Based on Figs. 8(a) and 8(b), the existence of 3rd and 5th PCC voltage harmonics results in increased peak-to-peak distortions of powers equal to 4 kW and 1 kVAR. For more clarity,

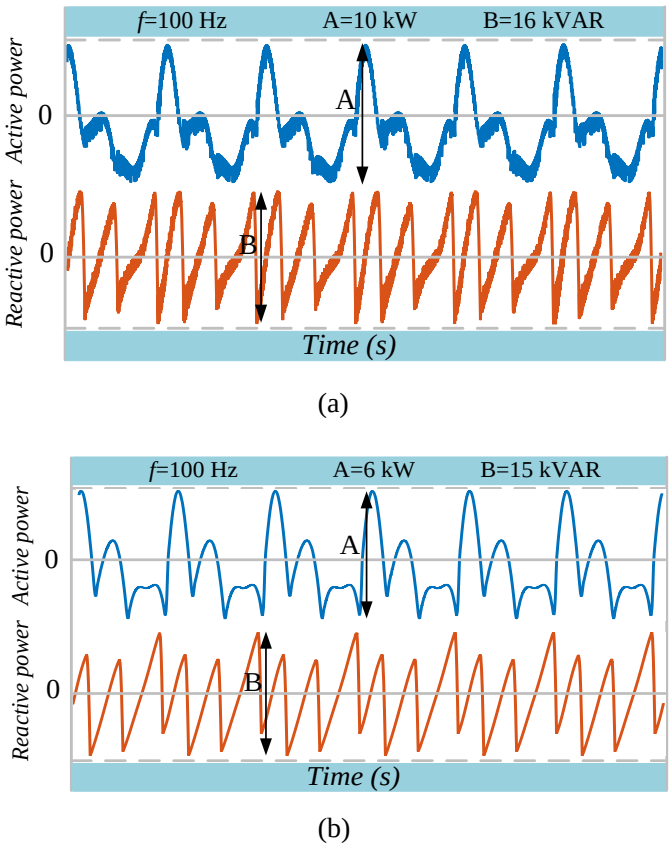

Fig. 8. The waveforms of total distortion powers, and (b) the waveforms of showing distortion contribution of NLLs (DC-NLLs)

the spectrum analysis of total distortion powers and DC-NLLs have been illustrated in Figs. 9(a) and 9(b), respectively, where the frequency of fundamental component is equal to 100 Hz, while the other components are the integer multiplier of 100 Hz. Note that the DC component of powers is in accordance with the fundamental of NLLs current, as well as the PCC voltage, filtered by LPFs. Using Figs. 9(a) and 9(b) and comparing the total distortion powers and DC-NLLs for both active and reactive distortion powers, the NLLs have less contribution. For 1st, 2nd, 3rd, 4th and 5th orders of active distortion powers, the PCC voltage harmonics have a greater effect on the distortion powers. In the DC-NLLs compensation mode, the grid-connecting VSC only rectifies the DC-NLLs of powers, as shown in Figs. 9(a) and 9(b). Difference between the total distortion powers and DC-NLLs denotes the DC-G, caused by the background voltage harmonics. It is obvious that the extracted DC-NLLs will be compensated by the suggested multifunctional control strategy; and as a result, the waveforms of VSC output and AC grid currents are obtained as Figs. 10(a) and 10(b). Note that in this mode, the microgrid VSC compensates the DC-NLLs while it injects the required powers. According to Fig. 10(a), the suggested control strategy supplies the powers with THD of 8.02%. In this situation, the AC grid is only subjected to THD of 6.53%, which is in accordance with the PCC voltage harmonics. Fig. 11 shows the power contribution and the compensation percentage of grid-connecting VSC in the DC-NLLs compensation mode

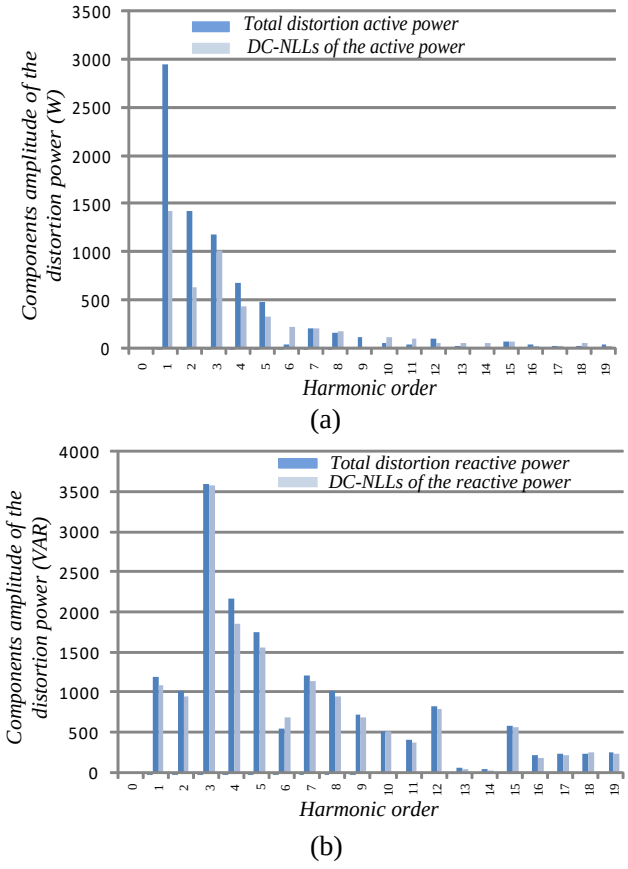

Fig. 9. The spectrum of total distortion power and DC-NLLs (a) active power, and (b) reactive power

B. Full Compensation Mode

The aim of this mode is full compensation; as a result, the AC grid will not be subjected to the any distortion. To this end, the suggested control strategy extracts the powers of DC-G, as depicted in Fig. 12. Note that DC-NLLs are similar to Fig. 8(b). Hence, the sum of these two distortion powers is exploited to generate the suitable reference signal for switching of the VSC. Based on Fig. 12, the PCC voltage harmonics produce a peak-to-peak distortion powers equal to 4.5 kW and 2 kVAR. The spectrum of total distortion powers and the powers of DC-G have been illustrated in Fig. 13. Accordingly, a part of total distortion powers is formed out of the powers of DC-G, which is relate to the PCC voltage harmonics. However, considering Fig. 9 and Fig. 13, a major part of the total distortion powers is

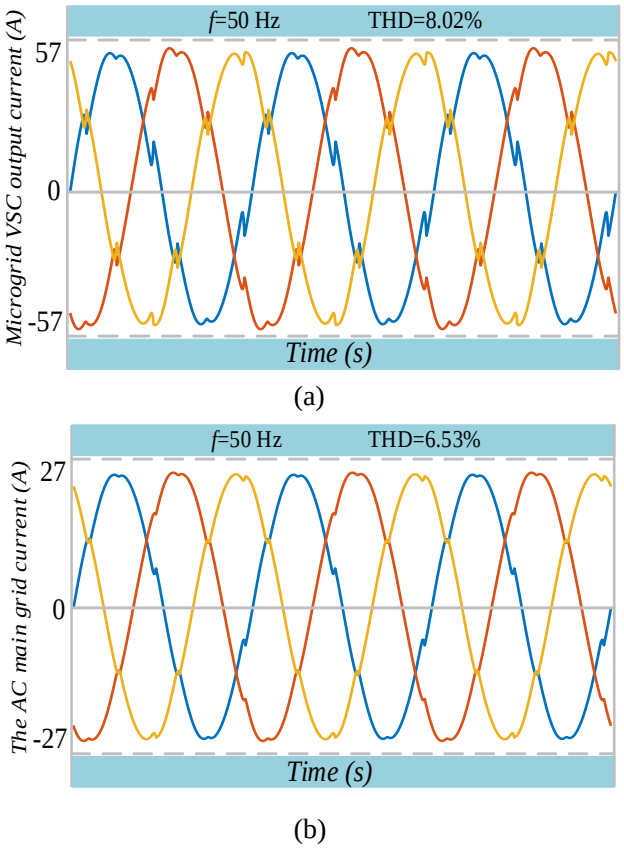

Fig. 10. The currents of (a) VSC output, and (b) grid

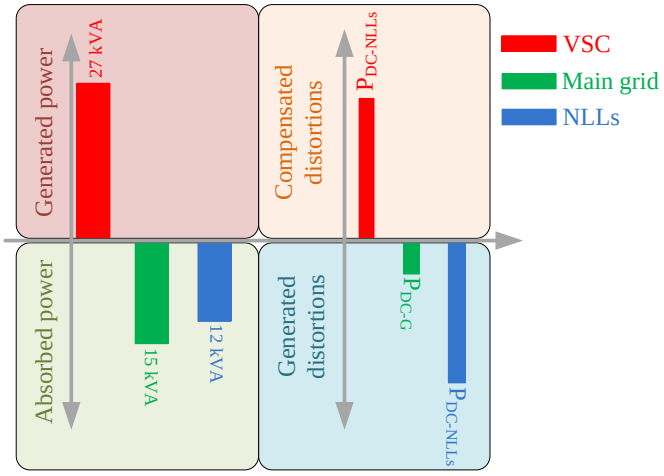

Fig. 11. Power contribution and compensation percentage in DC-NLLs compensation mode

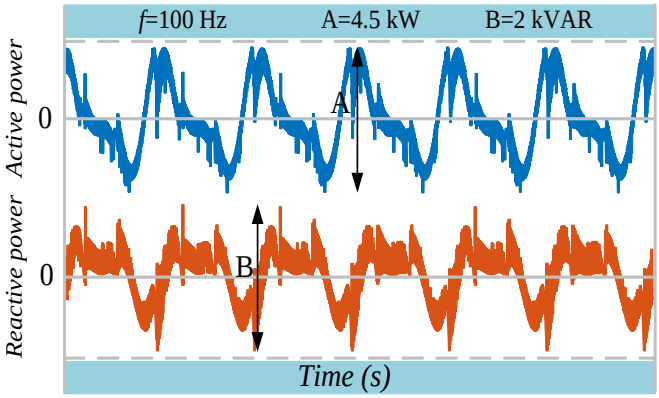

Fig. 12. The powers of main grid (DC-G)

the powers of DC-NLLs, but the effect of DC-G is not ignorable. Notably, in the presence of PCC voltage harmonics or NLLs, the powers of DC-G have more contribution in the total distortion powers. In full compensation mode, grid-connecting VSC deals with the compensation of total distortion powers or the sum of powers of DC-NLLs and DC-G. Thus, the current of AC grid will be compensated, while the VSC supplies the distortion powers of NLLs. The waveforms of VSC output and AC grid currents have been given in Fig. 14(a) and 14(b), respectively. Fig. 14(a) indicates that the microgrid VSC compensates the AC grid current by injecting current with THD of 9.82% in the full compensation mode. Hence, the THD of AC grid decreases to 1.65%, which is acceptable in the IEEE Standard 1547. In this mode, all distortion powers of NLLs, both powers of DC-NLLs and DC-G, are compensated by VSC. The summary of simulation results and the comparison of suggested control strategy with the previous works are listed in Table 2. Referring to Table 2, compared to previous control methods [19], [24] and [25], the proposed multifunctional control method has a better performance, and it can distinguish between the DC-NLLs and DC-G, while the other methods cannot realize this capability. According to this table, the suggested control approach has great function in comparison with previous methods in terms of distortions compensation of the grid-side current. However, some methods such as [26] and [27] have more functions including maximum power extraction from PV array and seamless transition from grid connected mode to standalone mode, but unlike these methods, the suggested control strategy can separate the distortions contribution of the NLLs and main grid, and as a result, compensation of these distortions can be accomplished by the proposed method in two modes. Nevertheless, in both [24] and [25], the control methods involve many functions that leads to increasing the complexity of control system. So, their implementation needs to high performance microcontrollers. Plus, the dynamic response and stability of system can be affected by the sophisticated control structures.

5. EXPERIMENTAL RESULTS

For validation of explained theory, as well as the provided simulation results, the prototype of grid-connecting microgrid VSC is implemented based on the suggested multifunctional control approach. To this end, the Texas TMS320F2812 microprocessor (DSP) is employed as a unit control. LV25-P and LEM-LA28-P voltage and current transducers have been employed in the hardware prototype to measure and generate suitable feedback. The required signals are sampled by transducers, and then are applied to the interfacing board for eliminating any noises. Further, the requirements of protection and signal shifting are accomplished by the interfacing board. Finally, after synthesizing the

Table 2. The simulation results and performance comparison of with similar control methods

Reference	Control method	THD of NLLs	THD-CGC *	Reduction percent	Ability for-DC-NLLs and DC-G-Separation
[19]	Optimized MPC	28.43%	2.66%	90.60%	No
[24]	PR	30.95%	6.37%	79.41%	No
[25]	VAM	23.63%	5.8%	75.45%	No
[26]	Multifunction	25%	5.5%	78%	No
[27]	VFXLMS	20.66%	3.99%	81%	No
proposed	multifunctional	32.60%	1.65%	94.93%	Yes

*THD of the compensated grid current.

voltage and current signals by the interfacing board, they are fed to the DSP board for generating suitable switching pulses of the IGBTs of VSC. The hardware of implemented microgrid VSC is shown in Fig. 15. Due to the limitation of the measurement tools, the waveforms of a single-phase of the three-phase system have been exhibited Both compensation modes are investigated. The single-phase waveforms of NLLs current and the PCC voltage have been depicted in Fig. 16(a), and their spectrum is demonstrated in Figs. 16(b) and 16(c), respectively. As can be seen from Fig. 16(b), NLLs absorb the current with the THD of 20.4%, where the THD of PCC voltage is equal to 8.3% according to Fig. 16(c). Hence, the distortions of PCC voltage will affect the distortions of NLLs. In other words, the THD of NLLs (20.4%) is not due to the behavior of NLLs, as the PCC voltage harmonics has an adverse effect on the THD of NLLs. In the DC-NLLs compensation mode, the current waveforms of VSC output and the AC grid have been illustrated in Figs. 17(a) and 17(b), respectively. In addition, Figs. 17(c) and 17(d) reveal the spectrum of VSC output and the AC grid currents, respectively. On the other hands, in the full compensation mode, the waveforms of VSC output and the AC grid currents have been depicted in Figs. 18(a) and 18(b), respectively. Eventually, the spectrum of currents of VSC output and the AC grid are demonstrated in Fig. 18(c) and 18(d), respectively. As can be seen in Fig. 17, in the DC-NLLs compensation mode, the microgrid VSC can compensate the distortion contribution of NLLs neglecting the effect of harmonics of PCC voltage. THD of the grid current is obtained 8.2%, where this value is in accordance with harmonics of PCC voltage. On the other hands, Fig. 18 shows that the suggested control strategy can compensate for all absorbed distortions of NLLs (considering the effect of harmonics of PCC voltage), and hence, the THD of AC grid is obtained 3.1%.

6. CONCLUSION

The paper has presented a novel multifunctional control approach for a grid-connecting microgrid VSC considering the main grid voltage harmonics. This new control method has been established based on the instantaneous power calculation instead of the evaluation of current harmonics of the NLLs. Due to the effect of the PCC voltage harmonics on the absorbed distortions by the local NLLs, the suggested control strategy can distinguish between the contribution of the PCC voltage harmonics, as well as the contribution of NLLs. Thus, through operation in the DC-NLLs compensation mode, the microgrid VSC has compensated the powers of the DC-NLLs neglecting the effect of the PCC voltage harmonics, and simultaneously, transferring the required powers.

On the other hand, in full compensation mode, the VSC has compensated all distortions created by the NLLs and PCC voltage harmonics. In this operation mode, the microgrid gains commercial benefit from the AC grid in ancillary service market because of the compensation of the distortion's contribution of the AC grid. The prominent feature of the suggested control strategy is its ability in separating the distortion contribution of the NLLs from the distortion contribution of the PCC voltage harmonics, and then their compensation in two selective modes. For validations of proposed control method, both simulations and experimental results have been presented in two operations modes. Based on experimental results, when the THD of main grid voltage distortions and absorbed current by NLLs are 8.3% and 20.4%respectively, the VSC based microgrid reduces the main grid side current THD equal to 8.2% and 3.1% in DC-NLLs and full compensation operation modes, respectively. These results prove the effectiveness of the proposed control method; however, its performance can be completed by adding new control loops for contribution to enhance of other phenomena such as balancing of grid, which can be investigated in future researches.

REFERENCES

1. E. Samavati and H. Mohammadi, "Simultaneous voltage and current harmonics compensation in islanded/grid-connected microgrids using virtual impedance concept," *Sustainable Energy, Grids and Networks*, vol. 20, p. 100258, 2019.
2. M. Fallah, H. M. Kojabadi, and F. Blaabjerg, "New control method for vsc-mtdc stations in the abnormal conditions of power system," *Control Engineering Practice*, vol. 96, p. 104316, 2020.
3. R. Ghanizadeh and G. B. Gharehpetian, "Distributed hierarchical control structure for voltage harmonic compensation and harmonic current sharing in isolated microgrids," *Sustainable Energy, Grids and Networks*, vol. 16, pp. 55–69, 2018.
4. D. Kanavaros, G. Oriti, and A. L. Julian, "Implementation and comparison of active and reactive power flow control methods in a single phase grid-connected microgrid," in *2019 IEEE Energy Conversion Congress and Exposition (ECCE)*, pp. 2800–2807, IEEE, 2019.
5. Y. Qi, P. Lin, Y. Wang, and Y. Tang, "Two-dimensional impedance-shaping control with enhanced harmonic power sharing for inverter-based microgrids," *IEEE Transactions on Power Electronics*, vol. 34, no. 11, pp. 11407–11418, 2019.
6. M. Fallah, H. M. Kojabadi, E. Pashajavid, A. N. Akpolat, and J. M. Guerrero, "Compensation of distortions in vsc-based dc–ac power systems using a modified vector control method," *Control Engineering Practice*, vol. 114, p. 104864, 2021.
7. A. Samadi, R. Eriksson, L. Söder, B. G. Rawn, and J. C. Boemer, "Coordinated active power-dependent voltage regulation in distribution

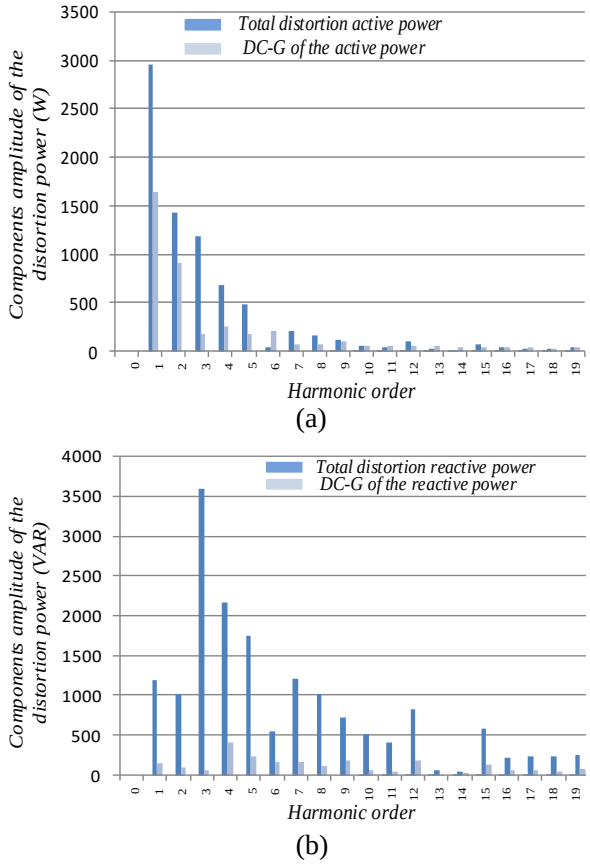

Fig. 13. The spectrum of total distortion power and DC-G (a) active, and (b) reactive

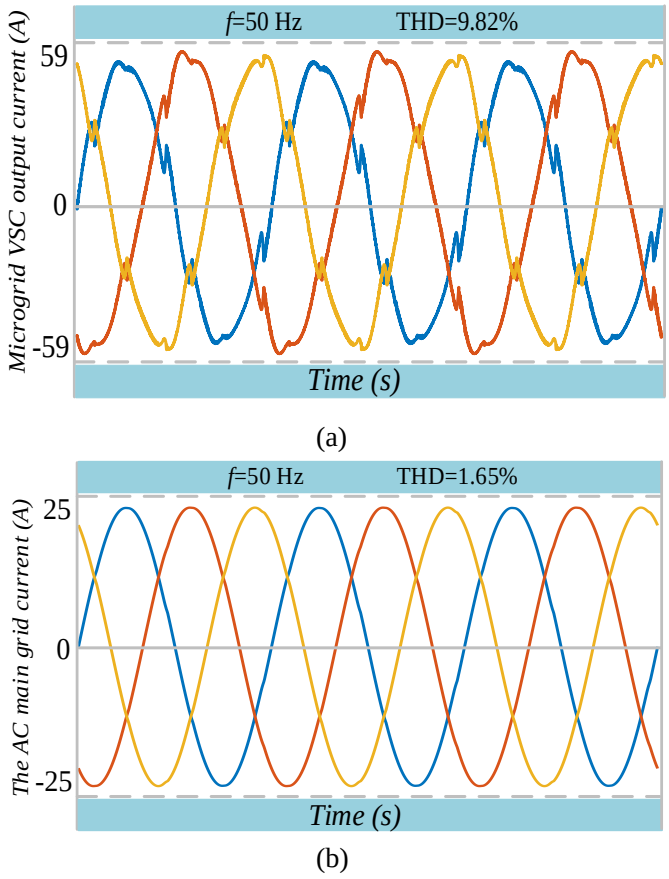

Fig. 14. The currents of (a) VSC, and (b) grid

grids with pv systems," *IEEE Transactions on power delivery*, vol. 29, no. 3, pp. 1454–1464, 2014.
8. A. R. Malekpour and A. Pahwa, "A dynamic operational scheme for residential pv smart inverters," *IEEE Transactions on Smart Grid*, vol. 8, no. 5, pp. 2258–2267, 2016.
9. R. Heydari, T. Dragicevic, and F. Blaabjerg, "High-bandwidth secondary voltage and frequency control of vsc-based ac microgrid," *IEEE Transactions on Power Electronics*, vol. 34, no. 11, pp. 11320–11331, 2019.
10. N. R. Tummuru, M. K. Mishra, and S. Srinivas, "Multifunctional vsc controlled microgrid using instantaneous symmetrical components theory," *IEEE Transactions on Sustainable Energy*, vol. 5, no. 1, pp. 313–322, 2013.
11. X. Zhao, L. Chang, R. Shao, and K. Spence, "Power system support functions provided by smart inverters—a review," *CPSS Transactions on Power Electronics and Applications*, vol. 3, no. 1, pp. 25–35, 2018.
12. J. He, Y. W. Li, F. Blaabjerg, and X. Wang, "Active harmonic filtering using current-controlled, grid-connected dg units with closed-loop power control," *IEEE Transactions on Power Electronics*, vol. 29, no. 2, pp. 642–653, 2013.
13. M. Fallah, J. Modarresi, H. M. Kojabadi, L. Chang, and J. M. Guerrero, "A modified indirect extraction method for a single-phase shunt active power filter with smaller dc-link capacitor size," *Sustainable Energy Technologies and Assessments*, vol. 45, p. 101039, 2021.
14. H. Joorabli, G. B. Gharehpetian, S. Ghassem-Zadeh, and V. Ghods, "A new control method for distortions compensation and power control using microgrid connecting voltage source converters," *Sustainable Energy Technologies and Assessments*, vol. 47, p. 101373, 2021.
15. H. Joorabli, G. Gharehpetian, Z. S. Ghassem, and V. Ghods, "Identification and determination of contribution of current harmonics and unbalanced in microgrids equipped with advanced metering infrastructure," 2021.
16. J. A. Rohten, J. J. Silva, J. A. Muñoz, F. A. Villarroel, D. N. Dewar, M. E. Rivera, and J. R. Espinoza, "A simple self-tuning resonant control approach for power converters connected to micro-grids with distorted voltage conditions," *IEEE Access*, vol. 8, pp. 216018–216028, 2020.
17. F. Hans, W. Schumacher, S.-F. Chou, and X. Wang, "Design of multi-frequency proportional–resonant current controllers for voltage-source converters," *IEEE Transactions on Power Electronics*, vol. 35, no. 12, pp. 13573–13589, 2020.
18. M. Zhu, Y. Ye, Y. Xiong, and Q. Zhao, "Parameter robustness improvement for repetitive control in grid-tied inverters using an iir filter," *IEEE Transactions on Power Electronics*, vol. 36, no. 7, pp. 8454–8463, 2020.
19. H. T. Nguyen and J.-W. Jung, "Disturbance-rejection-based model predictive control: Flexible-mode design with a modulator for three-phase inverters," *IEEE Transactions on Industrial Electronics*, vol. 65, no. 4, pp. 2893–2903, 2017.
20. M. Fallah, M. Imani, M. Abarzadeh, H. M. Kojabadi, and M. Hejri, "Load compensation based on frame considering low-order dominant harmonics and distorted power system," *Control Engineering Practice*, vol. 51, pp. 1–12, 2016.
21. M. Fallah, M. Imani, H. M. Kojabadi, M. Abarzadeh, M. T. Bina, and L. Chang, "Novel structure for unbalance, reactive power and harmonic compensation based on vff-rls and sogi-fll in three phase four wire power system," in *2015 IEEE Energy Conversion Congress and Exposition (ECCE)*, pp. 6254–6260, IEEE, 2015.
22. P. Rodríguez, J. Pou, J. Bergas, J. I. Candela, R. P. Burgos, and D. Boroyevich, "Decoupled double synchronous reference frame pll for power converters control," *IEEE Transactions on Power Electronics*, vol. 22, no. 2, pp. 584–592, 2007.
23. M. Fallah, R. Kazemzadeh, and H. Madadi Kojabadi, "Performance improvement of dvr using a new numerical lpf based on vff-rls and

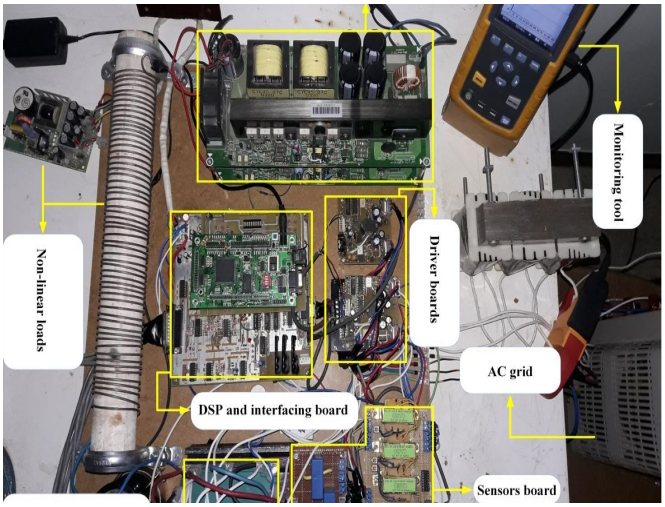

Fig. 15. The hardware of implemented microgrid VSC

fuzzy logic controller," *Journal of Vibration and Control*, vol. 24, no. 17, pp. 4037–4049, 2018.

24. G. Mirzaeva, G. C. Goodwin, B. P. McGrath, C. Teixeira, and M. E. Rivera, "A generalized mpc framework for the design and comparison of vsi current controllers," *IEEE Transactions on industrial electronics*, vol. 63, no. 9, pp. 5816–5826, 2016.
25. A. Micallef, M. Apap, C. Spiteri-Staines, and J. M. Guerrero, "Mitigation of harmonics in grid-connected and islanded microgrids via virtual admittances and impedances," *IEEE transactions on smart grid*, vol. 8, no. 2, pp. 651–661, 2015.
26. V. Narayanan, S. Kewat, and B. Singh, "Solar pv-bes based micro-grid system with multifunctional vsc," *IEEE Transactions on Industry Applications*, vol. 56, no. 3, pp. 2957–2967, 2020.
27. S. Kumar, B. Singh, U. Kalla, S. Singh, and A. Mittal, "Power quality control of small hydro-pv array and battery storage based microgrid for rural areas," in *2021 International Conference on Sustainable Energy and Future Electric Transportation (SEFET)*, pp. 1–6, IEEE, 2021.

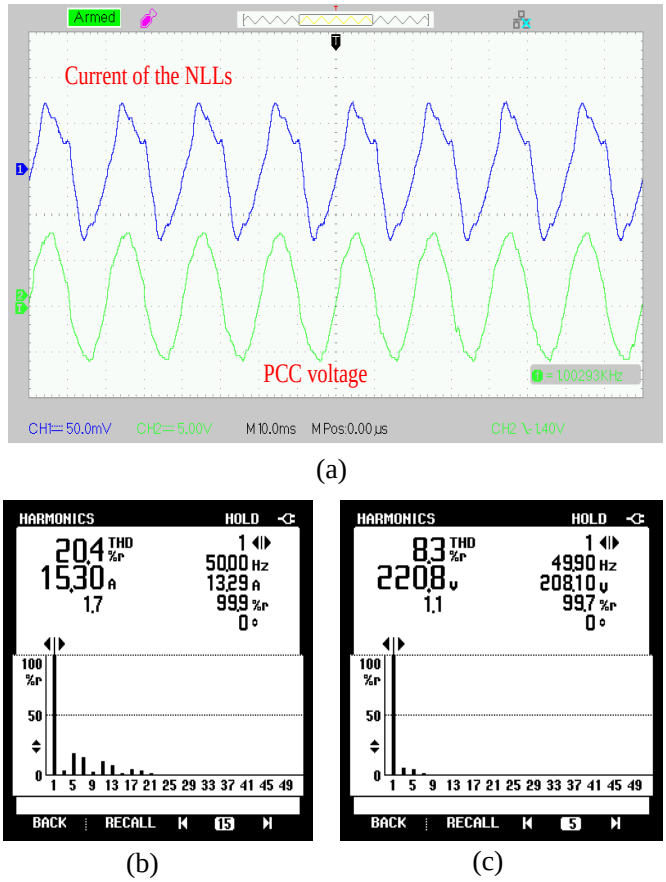

Fig. 16. (a) The waveforms of NLLs current (20A/div) and PCC voltage (200V/div), (b) NLLs current spectrum, and (c) PCC voltage spectrum

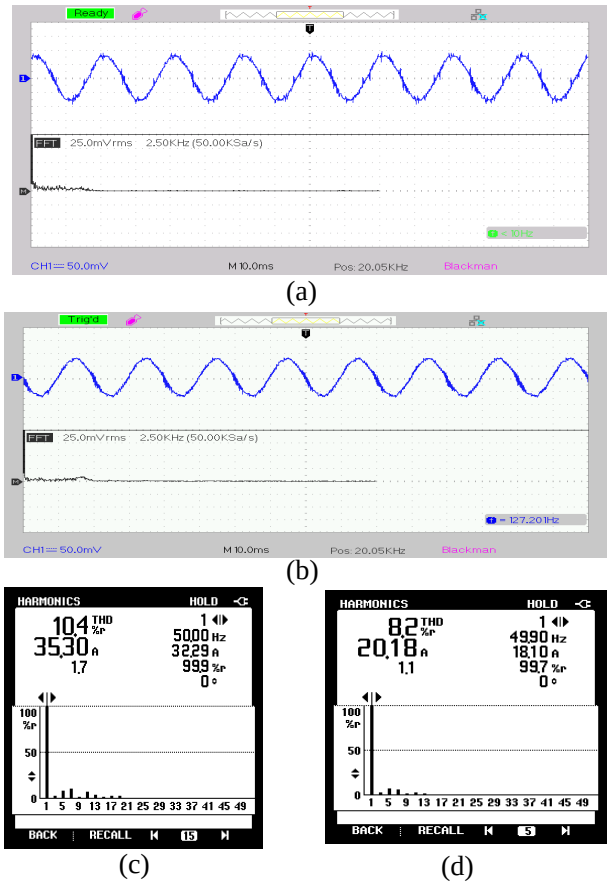

Fig. 17. In DC-NLLs compensation mode: (a) the waveform of VSC output current (40A/div), (b) grid current waveform (20A/div), (c) VSC output current spectrum, and (d) AC grid current spectrum

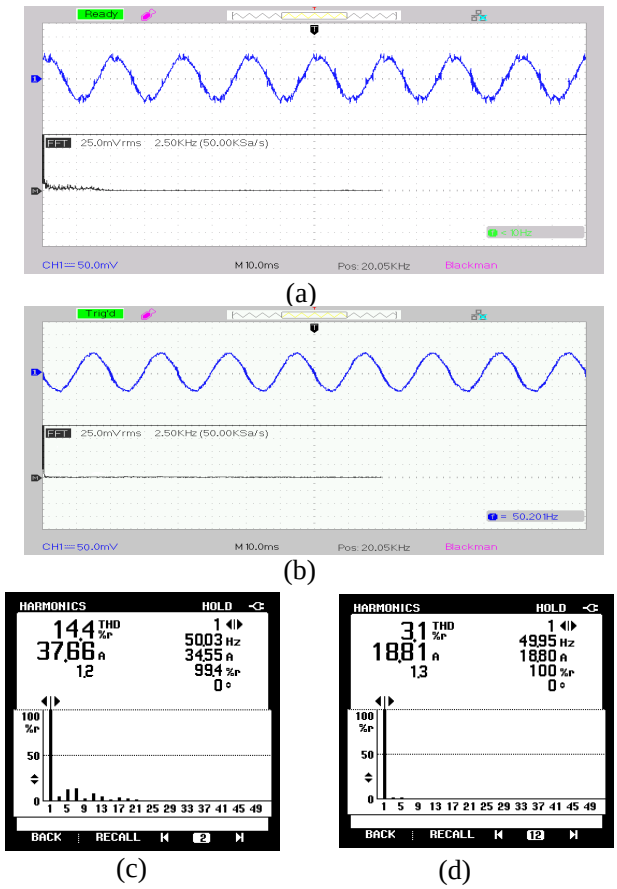

Fig. 18. In full compensation mode: (a) VSC output current waveform (40A/div), (b) AC grid current waveform (20A/div), (c) VSC output current spectrum, and (d) AC grid current spectrum